Journal of Power Sources 268 (2014) 482–490

Contents lists available at ScienceDirect

Journal of Power Sources

journal homepage: www.elsevier.com/locate/jpowsour

A thermal-electrochemical model that gives spatial-dependent growth of solid electrolyte interphase in a Li-ion battery

Lin Liu [a, 1], Jonghyun Park [a], Xianke Lin [a], Ann Marie Sastry [b], Wei Lu [a, *]

[a] Department of Mechanical Engineering, University of Michigan, Ann Arbor, MI 48109, USA
[b] Sakti3, Ann Arbor, MI 48108, USA

HIGHLIGHTS

- Integrated cell level thermal-electrochemical model with particle level SEI growth.
- Predicted spatial-dependent SEI growth in Li-ion batteries.
- SEI growth rate maximizes at the anode/separator interface.
- Higher temperature accelerates SEI growth, leading to more capacity loss.

GRAPHICAL ABSTRACT

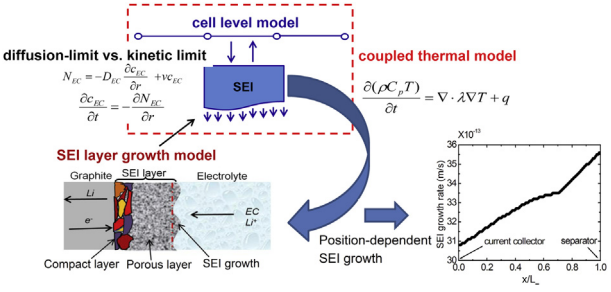

ARTICLE INFO

Article history:
Received 26 March 2014
Accepted 9 June 2014
Available online 18 June 2014

Keywords:
Li-ion batteries
SEI layer growth
Modeling
Thermal effects

ABSTRACT

The formation of a SEI layer and its growth cause internal resistance increase and capacity loss, leading to performance degradation of lithium-ion batteries. In order to comprehensively investigate the effects of SEI growth on battery performance, a one-dimensional thermal-electrochemical model was developed. This model is equipped with a growth mechanism of the SEI layer coupled with thermal evolution, based on the diffusional process of the solvent through the SEI layer and the kinetic process at the interface between the solid and liquid phases. The model is able to reveal the effects of diffusivity, reaction kinetics and temperature on SEI layer growth and cell capacity fade. We show that depending on the SEI thickness, the growth can be kinetics-limited or diffusion-limited. With the layer becoming thicker, its growth rate slows down gradually due to increased diffusion resistance. The SEI layer grows faster during charge than discharge due to the difference in the electron flux through the SEI layer and the temperature change during cycling. Temperature rise due to reaction and joule heating accelerates the SEI layer growth, leading to more capacity loss. Our model can provide insights on position-dependent SEI growth rate and be used to guide the strategic monitoring location.

1. Introduction

Aging is a significant concern in Lithium-ion Batteries (LIBs), especially in the application to electric vehicles (EVs) and hybrid EVs (HEVs) because of the requirement of cell durability [1,2]. Battery aging is caused by the material degradation of cell components and the introduction of new components by side reactions. It is well known that electrolyte decomposition, which is linked to the side reactions at electrode surfaces, yields a passivation film

* Corresponding author. Tel.: +1 734 647 7858; fax: +1 734 647 3170.
E-mail address: weilu@umich.edu (W. Lu).
[1] Current address: Department of Mechanical Engineering, University of Kansas, Lawrence, KS 66045, USA

http://dx.doi.org/10.1016/j.jpowsour.2014.06.050
0378-7753/

[3–5]. This film, referred as the solid electrolyte interface (SEI), suppresses further lithium corrosion and solvent decomposition [6,7]. Long-term stability of the SEI would have a prime impact on capacity retention, internal resistance and cyclability of LIBs. It has been reported that the long-term degradation of large-scale LIBs is caused by the formation and continuous growth of the SEI layer [8]. In spite of numerous research efforts, fundamental understanding of the SEI composition, stability, and its influence on battery performance is still controversial, and has been a focus of many researches over the past decade [9–13].

Developing appropriate laboratory aging tests to analyze the relation between SEI formation and cell aging is challenging. SEI growth involves a number of simultaneous physicochemical processes and their interactions [7,14–16]. Theoretical modeling and simulations are very useful to provide insight into the effects of SEI. Mathematical models have been developed to simulate the growth of SEI and lithium transport in the compact layer of SEI [9,17–19].

Advances in the understanding of SEI layer formation and growth call for a model to account for new observations. Research works suggest that the reductive electrolyte decomposition is accompanied by irreversible lithium ion consumption at the electrode/electrolyte interface. The products from decomposition and side reactions build up and form the SEI layer [7]. Some recent studies show that the SEI layer on the negative electrode material is composed of two distinct layers: a compact polycrystalline or heteromicrophase layer of inorganic products (e.g. Li_2CO_3, LiF, Li_2O, etc) and a porous amorphous outer layer composed of partially reduced organic products (e.g. $(CH_2OCO_2Li)_2$, ROLi, $ROCO_2Li$, etc) [20–26]. It is suggested that the outer layer of the SEI layer, whose pores are filled with electrolyte, controls the progress of SEI growth, and consequently the extent of capacity fade and internal resistance rise. The outer layer can be a couple of order of magnitudes thicker than the inner layer, while at the same time the outer layer is more vulnerable and unstable [23,27–29]. A recent work investigated the diffusion phenomena in the SEI porous layer and its growth [13]. However, the model was for a single particle.

SEI growth depends on the electron current flow and lithium diffusion, which vary at different locations in the electrode. A cell-level physics-based SEI growth model is necessary to reveal this spatial distribution of SEI and evaluate its effect on cell performance. Moreover, it is important to integrate the temperature effect in the cell-level model since it directly influences the material properties such as diffusivity and side reaction rates. Temperature is also of interest for the study of thermal runaway which is closely related to the safety of LIBs. Several cell-level thermal-electrochemical models were developed to investigate the temperature distribution and its effect on cell performance, however, SEI layer was either neglected or simplified as constant resistance in the battery system [30–32]. Thermal effect majorly impacts the side reaction for SEI formation and growth in the cell, while the thermal behavior of LIBs is in turn determined by the chemical and electrochemical processes occurring inside the cell during cycling [30]. Therefore, the SEI growth analysis needs to be coupled with the thermal effect.

In this paper a cell-level physics-based model is developed with the consideration of multiple key electrochemical processes, particularly the side reaction for continuous SEI growth and the thermal effect. The model has the potential to provide insights into the mechanisms related to capacity and power loss, as well as to reveal their effects on electric potential and Li ion concentration distribution. By considering solvent transport through the SEI porous layer [13], the model can capture lithium-ion diffusion and side reaction kinetics inside the layer. The model would also enable us to predict position-dependent SEI growth, providing important guidance for monitoring locations. In addition, this model considers the effect of SEI compact layer on lithium ion diffusion. SEI layer formation and growth are quite temperature-dependent. By incorporation of thermal energy conservation, the interaction between SEI layer growth and temperature, as well as their coupled effects on battery performance can be described. The model also considers double-layer capacity [33,34], which allows future electrochemical impendence spectroscopy (EIS) simulation. EIS simulation is a powerful tool to interpret Li ion and electron migration mechanisms, interfacial phenomenon, and failure mechanisms [35].

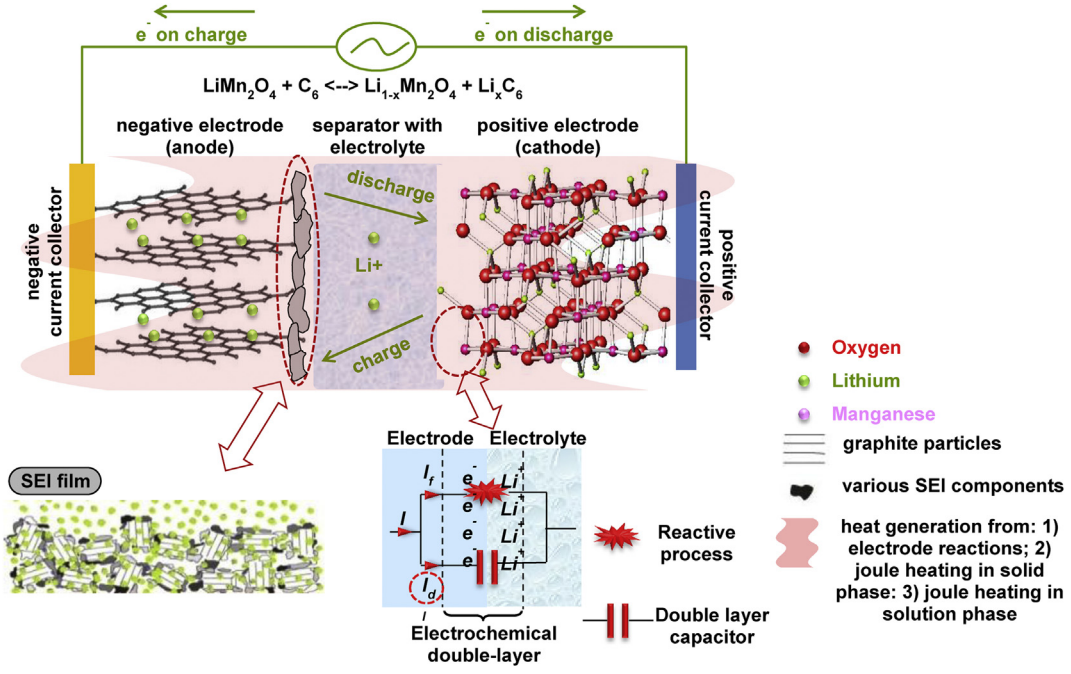

Fig. 1. A schematic showing the SEI layer, double-layer capacity and thermal effect in a lithium ion battery.

2. Model development

Fig. 1 shows a schematic of the SEI layer, double-layer capacity and thermal effect in a typical cell consisting of the current collector, anode, cathode, separator, and electrolyte solution. The SEI layer on the anode is much thicker compared to that on the cathode, which causes more rise in cell internal resistance and more capacity loss [36]. Therefore, here we focus on the SEI layer growth on the anode. SEI formation and growth reaction occurs continuously between the lithiated graphite and the electrolyte solvent. In the meanwhile, the growing SEI layer gradually consumes lithium and causes cell impedance increase during cycling. In this study the electrolyte solvent mixture contains ethylene carbonate (EC). The SEI is considered to be made of $(CH_2OCO_2Li)_2$, which has been shown to be a major component of the SEI porous layer [20–26]. The SEI formation process can be described by the following reactions [13].

$$EC + e^-(\text{graphite}) \rightarrow EC^- \tag{1}$$

$$EC^- + EC^- \rightarrow (O_2CO)^-(CH_2)_2(O_2CO)^- + C_2H_4\uparrow \tag{2}$$

$$EC^- + EC + e^-(\text{graphite}) \rightarrow (O_2CO)^-(CH_2)_2(O_2CO)^- + C_2H_4\uparrow \tag{3}$$

$$(O_2CO)^-(CH_2)_2(O_2CO)^- + 2Li^+ \rightarrow Li^+(O_2CO)^-(CH_2)_2(O_2CO)^-Li^+ \tag{4}$$

The double-layer capacity represents an additional mechanism to account for energy storage and the response to rapid current pulses. A modification to the regular current balance equations is needed to consider the charging of double layers in both anodes and cathodes [33,34]. The modification also appears in the mass balance equation for the electrolyte, since it includes the divergence of the current as a homogeneous source term. The thermal effect will be considered by a microscopic–macroscopic modeling approach.

2.1. 1D cell model

The charge conservation in the electrode and electrolyte phase can be described by

$$a_s i_{\text{loc}} = \frac{\partial i_2}{\partial x} - a_s C \frac{\partial(\phi_1 - \phi_2 - U - R_{\text{SEI}} i_{\text{loc}})}{\partial t} \tag{5}$$

$$i_2 = -\sigma_2^{\text{eff}} \frac{\partial \phi_2}{\partial x} + \frac{2RT\sigma_2^{\text{eff}}}{F}\left(1 + \frac{d\ln f_{\pm}}{d\ln c_2}\right)\left(1 - t_+^0\right)\frac{\partial \ln c_2}{\partial x} \tag{6}$$

$$a_s i_{\text{loc}} = \frac{\partial}{\partial x}\left(\sigma_1^{\text{eff}} \frac{\partial \phi_1}{\partial x}\right) \tag{7}$$

Equation (5) gives the intercalation current density in the porous electrode, where a_s is the active surface area per unit electrode volume and i_{loc} is the local current density. The first them on the right of Eq. (5) accounts for the divergence of the current flux in the electrolyte, where i_2 is the current density in the electrolyte phase. The second term accounts for the extra current due to the double layer capacity effect, where C is the double-layer capacitance, ϕ_1 is the electric potential of the solid phase, ϕ_2 is the electric potential of the liquid phase, U is the open-circuit potential that is dependent on the state of change (SOC), and R_{SEI} is the SEI layer resistance. In this study we focus on the SEI layer on the anode. The anode SEI resistance is estimated by $R_{\text{SEI}}(t) = \delta(t)/\sigma_{\text{SEI}}$, where $\delta(t)$ is the SEI thickness at time t and σ_{SEI} is the SEI ionic conductivity. The cathode SEI resistance is assumed zero since it is much thinner. In Eq. (6) the first term accounts for the current flux due to conductivity, and the second term accounts for the effect of potential variation due to concentration variation of the salt in the electrolyte, where σ_2^{eff} is the effective conductivity of the electrolyte, F is the Faraday's constant, R is the universal gas constant, T is temperature, $f_{\pm}$ is the activity coefficient of salt in the electrolyte phase, c_2 is the lithium concentration in the electrolyte, and t_+^0 is the transference number of lithium ion with respect to the solvent. Equation (7) gives the intercalation current density calculated from the solid phase, where σ_1^{eff} is the effective conductivity of the electrode and the current density in the solid phase is $i_1 = -\sigma_1^{\text{eff}}(\partial\phi_1/\partial x)$.

The material balance for the electrolyte in the solution phase is given by

$$\frac{\partial(\varepsilon_2 c_2)}{\partial t} = \frac{\partial}{\partial x}\left(D_2^{\text{eff}}\frac{\partial c_2}{\partial x}\right) + \frac{a_s i_{\text{loc}}}{F}\left(1 - t_+^0\right) + \frac{a_s C}{F}\left(1 - t_+^0\right)\frac{\partial(\phi_1 - \phi_2 - U - R_{\text{SEI}} i_{\text{loc}})}{\partial t} \tag{8}$$

where ε_2 is the electrode porosity or electrolyte phase volume fraction, and D_2^{eff} is the effective Li diffusion coefficient in the electrolyte. The last term on the right of Eq. (8) accounts for the extra salt storage variation over time in the solution phase due to the double layer capacity effect.

The diffusion of Li ions in an active solid particle is governed by the Fick's law

$$\frac{\partial c_1}{\partial t} = D_1\left(\frac{\partial^2 c_1}{\partial r^2} + \frac{2}{r}\frac{\partial c_1}{\partial r}\right) \tag{9}$$

where c_1 is the concentration of Li in the particle, r is the radial distance in the spherical coordinate and D_1 is the diffusion coefficient of Li in the solid.

The solid and solution phases are related by the boundary condition,

$$i_{\text{Li}} = -FD_1\frac{\partial c_1}{\partial r}\bigg|_{r=R_s} \tag{10}$$

where i_{Li} is the current density of Li intercalation into or deintercalation from graphite and R_s is the radius of the active material particle.

The intercalation current at cathode can be described by the Bulter–Volmer equation,

$$i_{loc} = i_{\text{Li}} = Fk_0 c_{1,s}^{\beta}(c_{1,\max} - c_{1,s})^{1-\beta} c_2^{1-\beta}\left\{\exp\left[\frac{(1-\beta)F}{RT}(\phi_1 - \phi_2 - U)\right] - \exp\left[-\frac{\beta F}{RT}(\phi_1 - \phi_2 - U)\right]\right\} \tag{11}$$

where k_0 is the rate coefficient for lithium intercalation reaction at cathode, β is the charge-transfer coefficient, $c_{1,s}$ is the Li concentration on the surface of the active material particle, and $c_{1,\max}$ is the maximum possible Li concentration in the active material.

2.2. SEI growth modulus

Here we extend SEI growth on the surface of a single particle to a thermal-electrochemical 1D cell-level model. The electrolyte

solution is $LiPF_6$ in EC/DMC. The compact SEI layer is assumed to be 1 nm thick ($L_{SEI}(0) = 1$ nm), which also accounts for an initial SEI layer resistance of $R_{SEI}(0) = 1\ \Omega\ cm^2$. The porous layer is assumed to grow above the compact layer. The dilute solution theory can be used to describe the flux of charged species in the SEI layer [37]. Using the Bulter–Volmer equation to describe the lithium intercalation/deintercalation current in the active materials occurring at the interface between the graphite and the SEI layer, we have

$$i_{Li} = Fk_0 c_{1,s}^{\beta}(c_{1,\max} - c_{1,s})^{1-\beta} c_2^{1-\beta}\left\{\exp\left[\frac{(1-\beta)F}{RT}(\phi_1 - \phi_2 - U - R_{SEI} i_{loc})\right] - \exp\left[-\frac{\beta F}{RT}(\phi_1 - \phi_2 - U - R_{SEI} i_{loc})\right]\right\} \quad (12)$$

where k_0 is the rate coefficient for lithium intercalation reaction at anode and β is the charge-transfer coefficient.

The rate determining step is considered to be the radical anion formation shown in Eq. (1). The side reaction takes place at the same interface of the lithium intercalation/deintercalation reaction, and the kinetic expression for this side reaction is in the form of a Tafel-like expression,

$$i_{side} = -Fk_{SEI} c_{EC}\left\{\exp\left[-\frac{\beta_{SEI} F}{RT}(\phi_1 - \phi_2 - R_{SEI} i_{loc})\right]\right\} \quad (13)$$

where k_{SEI} is the rate constant of side reaction for SEI formation, c_{EC} is the solvent concentration in the SEI layer, and β_{SEI} is the charge-transfer coefficient. Considering simultaneous lithium intercalation/deintercalation reaction and side reaction, we can write the local current density at anode,

$$i_{loc} = i_{Li} + i_{side} \quad (14)$$

Now we look at the solvent transport in the SEI porous layer. The rate of the electrolyte solution concentration change inside the SEI porous layer is compensated by the gradient of electrolyte solution flux density, N_{EC}, which can be described by

$$\frac{\partial c_{EC}}{\partial t} = -\frac{\partial N_{EC}}{\partial r} \quad (15)$$

Considering both diffusion and convection, the flux density is given by

$$N_{EC} = -D_{EC}\frac{\partial c_{EC}}{\partial r} + v c_{EC} \quad (16)$$

where D_{EC} is the diffusion coefficient and v is the velocity of the solvent relative to the SEI. The growth rate of the SEI layer due to the accumulation of lithium ethylene dicarbonate is related to the side reaction rate by

$$v = \frac{d\delta}{dt} = -\frac{i_{side}}{2F}\frac{M_{SEI}}{\rho_{SEI}} \quad (17)$$

where M_{SEI} is the molecular weight of the SEI and ρ_{SEI} is the density of the SEI.

Substitution of Eq. (16) to Eq. (15) gives the material balance in the SEI porous layer

$$\frac{\partial c_{EC}}{\partial t} = D_{EC}\frac{\partial^2 c_{EC}}{\partial r^2} - v\frac{\partial c_{EC}}{\partial r} \quad (18)$$

At the boundary between the SEI and the particle surface, the solvent flux matches the side reaction current, which gives

$$N_{EC}|_{r=R_s} = \frac{i_{side}}{F} \quad (19)$$

At the interface between the SEI and the solvent, the concentration is given by

$$c_{EC}|_{r=R_s+\delta} = \varepsilon_{SEI} c_{EC,0} \quad (20)$$

where ε_{SEI} is the SEI porosity and $c_{EC,0}$ is the solvent concentration in the bulk of the electrolyte.

The boundary conditions for the cell level model are

$$\left.\frac{\partial c_1}{\partial r}\right|_{r=0} = 0, \quad \left.\frac{\partial c_1}{\partial r}\right|_{r=R_s} = -\frac{i_{Li}}{FD_1}, \quad \left.\frac{\partial c_2}{\partial x}\right|_{x=0} = \left.\frac{\partial c_2}{\partial x}\right|_{x=L} = 0 \quad (21)$$

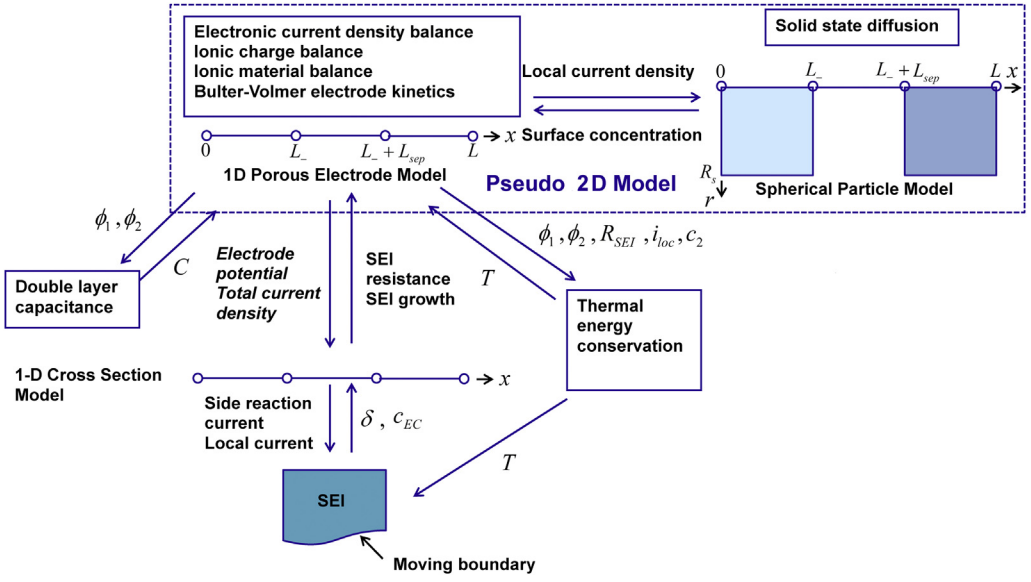

Fig. 2. Coupling of the models.

Table 1
Values of parameters used in the simulations.

Parameters	Anode	Cathode	Separator	SEI
Active surface area per unit electrode volume (m^{-1}), a_s[a]	113040	111375		
Cell area (m^2), A[a]	2.4×10^{-3}			
Maximum solid phase Li concentration (mol m^{-3}), $c_{1,max}$[a]	26390	22860		
Initial electrolyte salt concentration (mol m^{-3}), $c_2(0)$[a]	2000			
EC solution phase concentration (mol m^{-3}), $c_{CE,0}$[b]				4541
Double-layer capacitance (F m^{-2}), C[c]	0.1	0.1		
Heat capacity (J kg^{-1} K^{-1}), C_p[d]	700	700	700	
Solid phase Li diffusion coefficient (m^2 s^{-1}), D_1[a]	3.9×10^{-14}	1×10^{-13}		
Electrolyte phase Li diffusion coefficient (m^2 s^{-1}), D_2[a]	7.5×10^{-11}	7.5×10^{-11}	7.5×10^{-11}	
Effective electrolyte phase Li diffusion coefficient (m^2 s^{-1}), D_2^{eff}	$D_2^{eff} = D_2(\varepsilon_2)^p$			
EC diffusion coefficient (m^2 s^{-1}), D_{EC}[e]				1×10^{-13}
Activation energy for Li diffusion in solid phase (kJ mol^{-1}),$E_{act,D1}$[d]	4	20		
Activation energy for Li diffusion in electrolyte phase (kJ mol^{-1}),$E_{act,D2}$[d]	10			
Activation energy for exchange current density (kJ mol^{-1}),$E_{act,k0}$[d]	30	30		
Activation energy for SEI reaction rate (kJ mol^{-1}),$E_{act,kSEI}$[b]				200
Activation energy for electrolyte conductivity (kJ mol^{-1}), $E_{act,\sigma 2}$[d]	20			
Electrolyte activity coefficient,$f_{\pm}$[a]	1			
Faraday's constant (C mol^{-1}), F	96485.3			
Heat transfer coefficient (W m^{-2} K^{-1}), h[d]	5	5		
Reaction rate coefficient ($m^{4-3\beta}$ s^{-1} $mol^{\beta-1}$), k_0[a]	2×10^{-6}	2×10^{-6}		
SEI reaction rate coefficient (m s^{-1}), k_{SEI}[b]				1.37×10^{-5}
Electrode thickness (μm), L	100	183	52	
Initial SEI thickness (nm), $L_{SEI}(0)$[g]				1
SEI molar mass (kg mol^{-1}), M_{SEI}[f]				0.162
Bruggeman porosity exponent, p	1.5	1.5		
Gas constant (J mol^{-1} K^{-1}), R	8.314			
Particle radius (μm), R_s	12.5	8.5		
SEI initial resistance ($\Omega \cdot cm^2$), $R_{SEI}(0)$[f]				1
Initial state of charge, SOC	0.56347	0.1706		
Li transference number,t_+^0[a]	0.363	0.363	0.363	
Environmental temperature (K), T_0	298.15			
Open circuit potential (V), U[a]	U_-	U_+		
$U_- = -0.16 + 1.32\exp(3.0x) + 10.0\exp(-2000.0x)$ for Li_xC_6, $x = c_{1,s}/c_{1,max}$ at anode				
$U_+ = 4.19829 + 0.0565661\tanh[-14.5546y + 8.60942] - 0.0275479[1/(0.998432 - y)^{0.492465} - 1.90111] - 0.157123\exp(0.04738y^8) + 0.810239\exp[-40(y - 0.133875)]$ for $Li_yMn_2O_4$, $y = c_{1,s}/c_{1,max}$ at cathode				
Entropy change of the electrode reaction (V K^{-1}), $\partial U/\partial T$[d]	0	0		
Charge transfer coefficient, β[a]	0.5	0.5		
SEI charge transfer coefficient, β_{SEI}[g]				0.5
Solid phase volume fraction,ε_1[a]	0.471	0.297		
Electrolyte phase volume fraction, ε_2[a]	0.357	0.444	1	
SEI Porosity, ε_{SEI}[f]				0.05
Thermal conductivity (W m^{-1} K^{-1}), λ[d]	5	5	1	
Mass density (kg m^{-3}), ρ[d]	2.5×10^6	1.5×10^6	1.2×10^6	
SEI density (kg m^{-3}), ρ_{SEI}[f]				1.69×10^3
Solid phase conductivity (S m^{-1}),σ_1[a]	100	3.8		
Effective solid phase conductivity (S m^{-1}), σ_1^{eff}	$\sigma_1^{eff} = \sigma_1(\varepsilon_1)^p$			
Electrolyte phase ionic conductivity (S m^{-1}), σ_2[a]				
$\sigma_2 = 1.0793 \times 10^{-2} + 6.7461 \times 10^{-4}c_2 - 5.2245 \times 10^{-7}(c_2)^2 + 1.3605 \times 10^{-10}(c_2)^3 - 1.1724 \times 10^{-14}(c_2)^4$				
Effective electrolyte phase ionic conductivity (S m^{-1}), σ_2^{eff}	$\sigma_2^{eff} = \sigma_2(\varepsilon_2)^p$			
Effective electrolyte phase diffusional conductivity (A m^{-1}), σ_{2D}^{eff}	$\sigma_{2D}^{eff} = \frac{2RT\sigma_2^{eff}}{F}(1 - t_+^0)\left(1 + \frac{d\ln f_\pm^+}{d\ln c_2}\right)$			
SEI ionic conductivity (S m^{-1}), σ_{SEI}[f]				5×10^{-6}

[a] Data from Ref. [41].
[b] Data from Ref. [12].
[c] Data from Ref. [34].
[d] Data from Ref. [39].
[e] Data from Ref. [17].
[f] Data from Ref. [13].
[g] Assumed.

$$-\sigma_1^{\text{eff}}\frac{\partial\phi_1}{\partial x}\bigg|_{x=0} = \sigma_1^{\text{eff}}\frac{\partial\phi_1}{\partial x}\bigg|_{x=L} = \frac{I}{A}, \quad \frac{\partial\phi_1}{\partial x}\bigg|_{x=L_-} = \frac{\partial\phi_1}{\partial x}\bigg|_{x=L_-+L_{\text{sep}}} = 0, \quad \frac{\partial\phi_2}{\partial x}\bigg|_{x=0} = \frac{\partial\phi_2}{\partial x}\bigg|_{x=L} = 0 \tag{22}$$

where L is the thickness of the cell, I is the cell current, A is the cross-section area of the cell, L_- is the thickness of the anode, and L_{sep} is the thickness of the separator.

2.3. Thermal modulus

The thermal energy conservation can be expressed by

$$\frac{\partial(\rho C_p T)}{\partial t} = \nabla\cdot\lambda\nabla T + q \tag{23}$$

where ρ is the mass density, C_p is the heat capacity, and λ is the thermal conductivity of the cell component. The heat generation rate per unit volume, q, can be expressed by Refs. [38,39],

$$q = a_s i_{\text{loc}}\left(\phi_1 - \phi_2 - U - R_{\text{SEI}} i_{\text{loc}} + T\frac{\partial U}{\partial T}\right) + \sigma_1^{\text{eff}}(\nabla\phi_1)^2 + \sigma_2^{\text{eff}}(\nabla\phi_2)^2 + \sigma_{2D}^{\text{eff}}\nabla\ln c_2\cdot\nabla\phi_2 \tag{24}$$

where σ_{2D}^{eff} is the effective solution phase diffusional conductivity. Here, the first term of the right-hand side represents the heat sources due to charge transfer at the electrode/electrolyte interfaces and the entropy change. The last two terms arise from the joule heating in the solid active and electrolyte phases, respectively. The boundary conditions are given at $x = 0$ and $x = L$ by $-\lambda\nabla T = h(T-T_0)$, where T_0 is the environmental temperature, and h is the heat transfer coefficient.

The temperature-dependent physicochemical properties are descripted by the Arrhenius equation,

$$\Phi = \Phi_{\text{ref}}\exp\left[\frac{E_{\text{act},\Phi}}{R}\left(\frac{1}{T_{\text{ref}}} - \frac{1}{T}\right)\right] \tag{25}$$

where Φ is a general variable that represents the diffusion coefficient of a species, the conductivity of the electrolyte, or the exchange current density of an electrode reaction, etc., with the subscript ref indicating the value at a reference temperature. E_{act} is the corresponding activation energy.

We developed our multi-scale and multi-physics model using the COMSOL Multiphysics 4.2a software. Fig. 2 shows the coupling among the components. The 1D porous electrode model is composed of the anode region ($0 \le x \le L_-$), the separator region ($L_- \le x \le L_- + L_{\text{sep}}$), and the cathode region ($L_- + L_{\text{sep}} \le x \le L$). To couple the 1D model with the Li^+ diffusion in the spherical solid particle, we add a vertical axis, r, to form a pseudo 2D model. This vertical axis denotes the radial direction of the solid particles. In the two dimensional (x, r) space, the Li^+ diffusion coefficient in the x direction is set to several orders of magnitude lower than that in the r direction to accomplish the radial diffusion descried by Eq. (9). The current flux calculated from the 1D model is projected to the lower $r = R_s$ boundary in Fig. 2, to solve the Li^+ concentration, c_1, in the solid particle phase. The solved concentration is then projected back to the 1D model to provide the surface concentration of the solid particle phase. Similarly, the SEI growth is performed in the pseudo 2D configuration and then projected back to the 1D model to provide the resistance of the SEI layer.

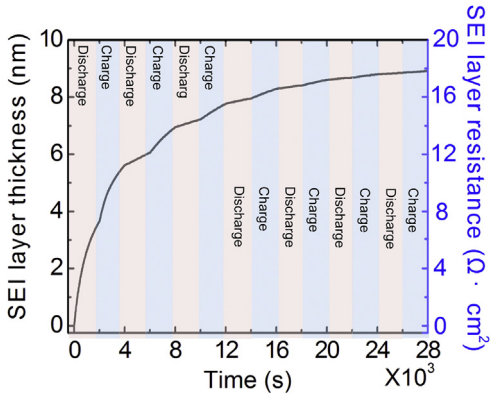

Fig. 3. SEI layer growth and its resistance reach a stable state after 7 cycles at the charge/discharge rate of 1C. SEI layer grows faster during charge than during discharge.

3. Results and discussion

The values of the parameters used in the simulations are listed in Table 1. Our model has the transient feature and can provide the capability to evaluate SEI growth during charge and discharge cycles. An initial SEI layer thickness of 1 nm was assumed to account for the SEI compact layer. The compact layer was assumed to form during the first charge of the cell to a SOC of 56%. The porous SEI layer formed and grew outside the compact layer. The growth of the porous layer is very sensitive to the diffusion process and the side reaction rate. Fig. 3 shows the SEI layer growth and the increase in layer resistance during the first seven cycles at 1C charge/discharge rate. After the initial discharge process, the SEI layer grows by 3.8 nm. During the next charge and discharge cycles, the SEI layer grows by 2 nm and 0.6 nm, respectively. The growth continuously slows down during further cycling. After seven cycles the thickness of the SEI porous layer increases to around 9 nm while its resistance rises to 18 Ω cm^2. Our simulations suggest that the SEI porous layer grows quickly toward the equilibrium thickness. This trend agrees with the reports [9,13,17,40] showing that SEI growth tends to slow down due to possible difficulty in electrolyte solution diffusion or high electrical resistance resulted from the SEI layer. Fig. 3 also shows that the SEI layer grows faster during charge than during discharge, which is consistent with experimental observations [9]. The growth rate is determined by the electron flux through the SEI layer. During charge, the injection of electrons into the anode makes it easier to leave the graphite and react with electrolyte and lithium ions to form SEI. The difference of growth rate during charge and discharge may also be related to the temperature. Fig. 4

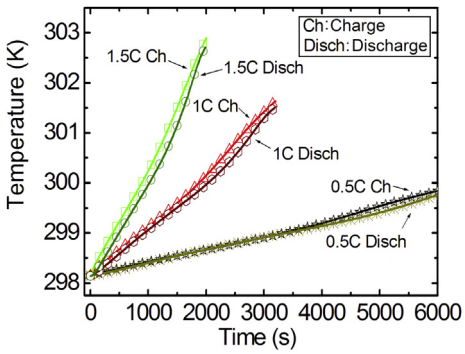

Fig. 4. A higher C-rate leads to more temperature increase. At the same C-rate, the temperature during charge is a litter higher than that during discharge.

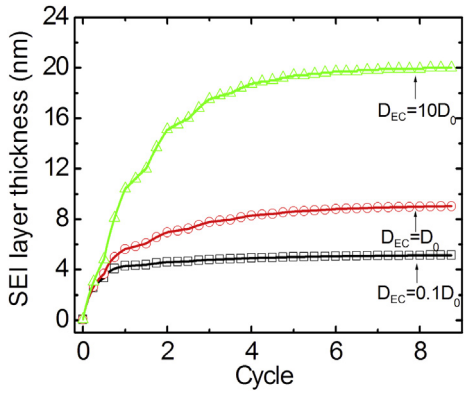

Fig. 5. Effect of electrolyte diffusion coefficient on SEI growth.

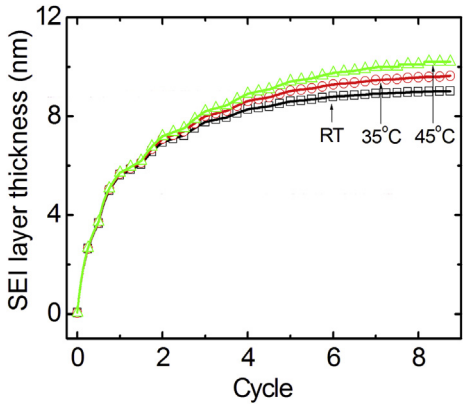

Fig. 7. Effect of environmental temperature on SEI growth.

shows that the temperature is slightly higher during charge than discharge, and the difference becomes more noticeable as the C-rate becomes larger. SEI grows faster at a higher temperature.

It is important to understand the relationship among diffusivity, side reaction rate, and SEI layer growth characteristics. When the diffusion coefficient is small, the system becomes diffusion-limited. Fig. 5 shows the SEI layer growth with different diffusion coefficients for the electrolyte in the SEI layer. With the diffusion coefficients increased by 2 orders of magnitude, which is consistent with the possible range reported in the literatures [13,41], the SEI layer grows 5 times as thick. With a lower diffusion coefficient, the SEI layer tends to reach its stable state faster but at a thinner thickness. For example, the SEI layer stops growth at cycle 2 and reaches a thickness of 4 nm with $D_{EC} = 0.1D_0$, where D_0 is the baseline value given in Table 1. If the diffusion coefficient rises by 2 orders of magnitude, the SEI layer reaches a stable state at around cycle 7 or 8 with a larger thickness of 20 nm. With a higher diffusion coefficient, the electrolyte solution penetrates through the SEI porous structure more easily to reach the reaction sites. Therefore, the SEI layer grows faster and thicker. The SEI layer growth also depends on its kinetic reaction. With a large diffusion coefficient, the system becomes more kinetics-limited. Fig. 6 shows the effect of side reaction rate constant on SEI growth. k_0 is the baseline value given in Table 1. The reaction rate can vary 2–3 orders of magnitude depending on the system [9,13]. With a faster reaction rate, the SEI layer grows faster and thicker, but takes a longer time to reach the stable thickness. The overall trend is that the SEI grows quickly in the first few cycles. The initial growth of SEI is kinetics-limited. The growth rate gradually slows down due to the rising diffusional resistance from the layer thickness, making the system shift toward diffusion-limited.

The performance of LIBs can be significantly influenced by temperature and the thermal behavior, which is also closely related to battery safety. While the thermal process can accelerate the electrochemical and chemical processes in LIBs, they also cause problems such as more internal resistance increase and capacity loss due to faster decomposition of the electrolyte and SEI growth. Fig. 7 shows the temperature effect on SEI growth. With a higher environmental temperature, the side reaction kinetics and diffusion accelerate, resulting in a thicker SEI layer. At 45 °C, the SEI thickness increases by more than 15% in the first 8 cycles comparing to that at room temperature. Previous studies have suggested that a higher temperature will accelerate the diffusion process [39,42]. Here we show quantitatively how temperature

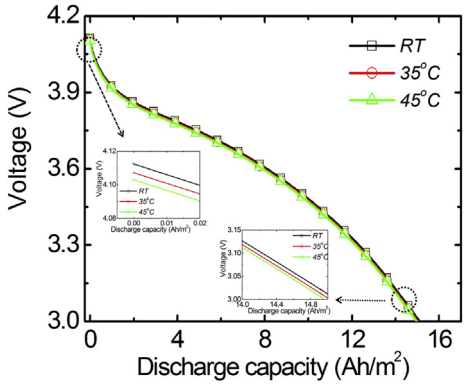

Fig. 8. A higher environmental temperature leads to more ohmic loss and capacity loss due to SEI growth.

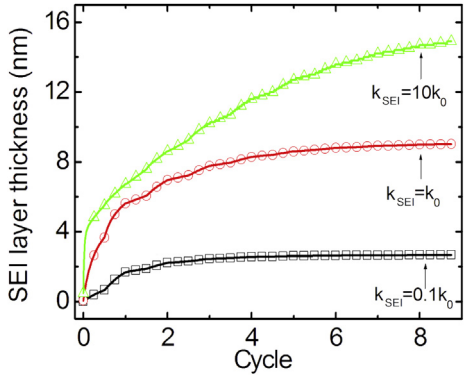

Fig. 6. Effect of side reaction rate constant on SEI growth.

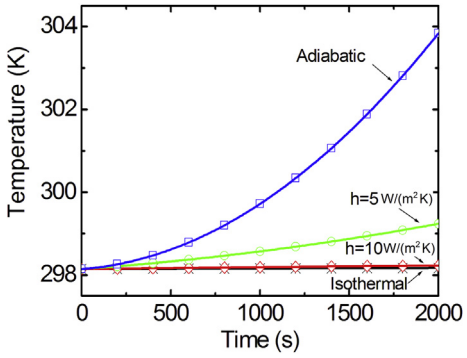

Fig. 9. Effect of boundary heat transfer on cell temperature.

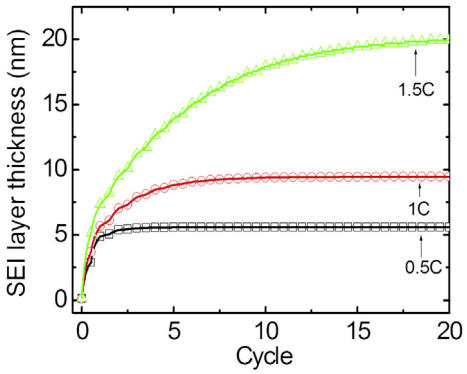

Fig. 10. Effect of C-rate on SEI growth.

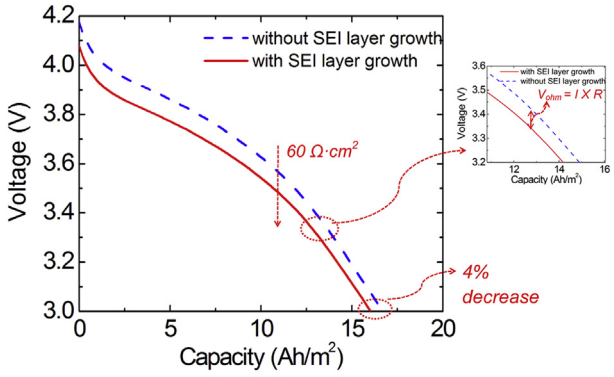

Fig. 11. Discharge profile at 1C with and without SEI growth.

affects the SEI growth. The resulting increase of internal resistance due to a thicker SEI leads to more ohmic and capacity loss, as shown in Fig. 8. We have investigated the increase of cell average temperature as a result of different boundary conditions, as shown in Fig. 9. With a higher thermal transfer coefficient, the increase in cell average temperature is negligible. However, as the cooling condition becomes worse, the cell temperature rises dramatically. As we have shown, higher temperature results in more ohmic loss and capacity loss. Therefore, temperature control is critical in cell performance. C-rate is another important parameter in determining SEI layer growth and cell performance. Fig. 10 shows the effect of C-rate on SEI growth. The SEI layer grows almost 4 times

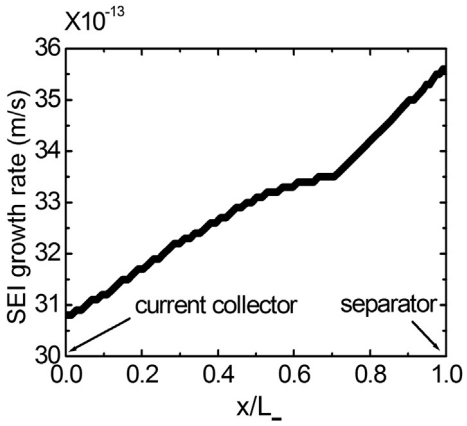

Fig. 12. Position-dependent SEI growth. The growth rate is higher at the anode/separator interface.

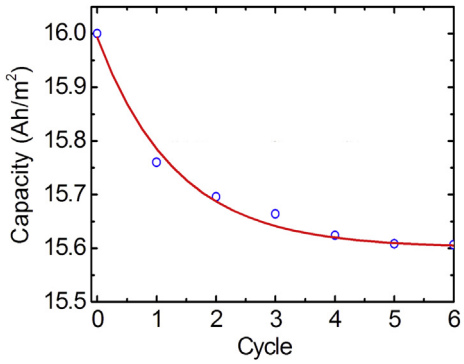

Fig. 13. Cell capacity decease during cycling as a result of SEI growth.

as thick when the C-rate is increased from 0.5C to 1.5C, which implies that the SEI layer growth is highly dependent on the current flow density inside the cell. The increase of internal resistance and capacity loss due to SEI growth will result in the degradation in cell performance. Fig. 11 shows the comparison of discharge profile at 1C with and without SEI growth. The SEI layer resistance increases to around 60 Ω cm^2 after 10 cycles, which causes about 4% capacity loss. The voltage drop mainly comes from the increased cell internal resistance associated with the SEI growth. The SEI growth depends on electron current flow and lithium diffusion, which varies at different locations in the electrode. A cell-level SEI growth model can reveal position-dependent SEI growth, which can be used as guidance for the location of monitoring. Fig. 12 shows the SEI growth rate along the anode thickness direction. The SEI layer grows faster at the interface between the anode and the separator ($x = L\_$) than at the current collector side ($x = 0$). The non-uniform SEI growth can result in uneven resistance increase and degradation in the cell, which may result in temperature increase and even thermal runaway. Fig. 13 shows the capacity loss due to SEI growth. The capacity loss stabilizes when the SEI layer reaches its stable thickness. The SEI layer reaches its stable state fairly quickly due to the slowdown of the diffusion and kinetic reaction processes, which is consistent with several observations [15,40,43].

4. Conclusions

In this study a cell-level physics-based model has been developed to couple the SEI layer growth and the thermal effect. The model provides an effective tool to investigate and evaluate the effects of SEI layer growth and temperature increase on the performance of LIBs. Depending on the processes of diffusion and side reaction, the SEI layer grows quickly to the stable state in the first several cycles. The slowing down of the SEI layer growth can be attributed to the difficulty in the diffusion process. The SEI growth under charge and discharge conditions shows different rates due to the electron flux difference through the SEI layer and temperature change during cycling. The SEI growth rate shows position dependence in the cell since the current flow and lithium diffusion vary at different locations in the electrode. The SEI grows faster at the interface between the anode and the separator, which is the strategic location for battery health monitoring in the battery control algorithm. The effect of environmental temperature and C-rate on SEI layer growth has also been investigated in this study. In the future, we plan to expand the model to perform EIS simulation, and to couple additional degradation mechanisms, such as lithium plating and manganese deposition. The model framework can be used as an effective tool for designing and optimizing the cell performance.

Acknowledgments

This research was funded by the GM/UM Advanced Battery Coalition for Drivetrains. Support from our sponsor is gratefully acknowledged.

References

[1] M. Woon, X. Lin, A. Ivanco, A. Moskalik, C. Gray, Z.S. Filipi, in, SAE International, 2011.
[2] X. Lin, A. Ivanco, Z. Filipi, SAE Int. J. Altern. Powertrains 1 (2012) 249–259.
[3] D. Aurbach, Y. Ein-Eli, B. Markovsky, A. Zaban, S. Luski, Y. Carmeli, H. Yamin, J. Electrochem. Soc. 142 (1995) 2882–2890.
[4] R. Imhof, P. Novak, J. Electrochem. Soc. 146 (1999) 1702–1706.
[5] D.H. Jang, Y.J. Shin, S.M. Oh, J. Electrochem. Soc. 143 (1996) 2204–2211.
[6] E. Peled, J. Electrochem. Soc. 126 (1979) 2047–2051.
[7] J. Vetter, P. Novák, M.R. Wagner, C. Veit, K.C. Möller, J.O. Besenhard, M. Winter, M. Wohlfahrt-Mehrens, C. Vogler, A. Hammouche, J. Power Sources 147 (2005) 269–281.
[8] M.I. Zempachi Ogumi, Carbon anodes, in: B.S. Walter, A. van Schalkwijk (Eds.), Advances in Lithium-ion Batteries, Kluwer Academic, New York, 2002, p. 97.
[9] A.M. Colclasure, K.A. Smith, R.J. Kee, Electrochim. Acta 58 (2011) 33–43.
[10] D. Aurbach, K. Gamolsky, B. Markovsky, G. Salitra, Y. Gofer, U. Heider, R. Oesten, M. Schmidt, J. Electrochem. Soc. 147 (2000) 1322–1331.
[11] D. Aurbach, B. Markovsky, M.D. Levi, E. Levi, A. Schechter, M. Moshkovich, Y. Cohen, J. Power Sources 81–82 (1999) 95–111.
[12] H.J. Ploehn, P. Ramadass, R.E. White, J. Electrochem. Soc. 151 (2004) 456–462.
[13] M. Safari, M. Morcrette, A. Teyssot, C. Delacourt, J. Electrochem. Soc. 156 (2009) 145–153.
[14] S.-P. Kim, A.C.T.v. Duin, V.B. Shenoy, J. Power Sources 196 (2011) 8590–8597.
[15] K.C. Möller, H.J. Santner, W. Kern, S. Yamaguchi, J.O. Besenhard, M. Winter, J. Power Sources 119–121 (2003) 561–566.
[16] M. Park, X. Zhang, M. Chung, G.B. Less, A.M. Sastry, J. Power Sources 195 (2010) 7904–7929.
[17] J. Christensen, J. Newman, J. Electrochem. Soc. 151 (2004) A1977–A1988.
[18] S.Q. Shi, P. Lu, Z.Y. Liu, Y. Qi, L.G. Hector, H. Li, S.J. Harris, J. Am. Chem. Soc. 134 (2012) 15476–15487.
[19] X.K. Lin, J. Park, L. Liu, Y. Lee, A.M. Sastry, W. Lu, J. Electrochem. Soc. 160 (2013) A1701–A1710.
[20] J. Yan, B.-J. Xia, Y.-C. Su, X.-Z. Zhou, J. Zhang, X.-G. Zhang, Electrochim. Acta 53 (2008) 7069–7078.
[21] M. Tang, S.D. Lu, J. Newman, J. Electrochem. Soc. 159 (2012) A1775–A1785.
[22] J. Yan, J. Zhang, Y.-C. Su, X.-G. Zhang, B.-J. Xia, Electrochim. Acta 55 (2010) 1785–1794.
[23] A.M. Andersson, A. Henningson, H. Siegbahn, U. Jansson, K. Edström, J. Power Sources 119–121 (2003) 522–527.
[24] P. Ganesh, P.R.C. Kent, D.E. Jiang, J. Phys. Chem. C 116 (2012) 24476–24481.
[25] P. Lu, S.J. Harris, Electrochem. Commun. 13 (2011) 1035–1037.
[26] H.L. Zhang, F. Li, C. Liu, J. Tan, H.M. Cheng, J. Phys. Chem. B 109 (2005) 22205–22211.
[27] D. Bar-Tow, E. Peled, L. Burstein, J. Electrochem. Soc. 146 (1999) 824–832.
[28] D. Aurbach, Y. Ein-Eli, O. Chusid, Y. Carmeli, M. Babai, H. Yamin, J. Electrochem. Soc. 141 (1994) 603–611.
[29] S.-K. Jeong, M. Inaba, T. Abe, Z. Ogumi, J. Electrochem. Soc. 148 (2001) A989–A993.
[30] W.B. Gu, C.Y. Wang, J. Electrochem. Soc. 147 (2000) 2910–2922.
[31] L. Cai, R.E. White, J. Power Sources 196 (2011) 5985–5989.
[32] G.-H. Kim, K. Smith, K.-J. Lee, S. Santhanagopalan, A. Pesaran, J. Electrochem. Soc. 158 (2011) A955–A969.
[33] I.J. Ong, J. Newman, J. Electrochem. Soc. 146 (1999) 4360–4365.
[34] M. Doyle, J.P. Meyers, J. Newman, J. Electrochem. Soc. 147 (2000) 99–110.
[35] R.W.J.M. Huang, F. Chung, E.M. Kelder, J. Electrochem. Soc. 153 (2006) A1459–A1465.
[36] J. Lei, L. Li, R. Kostecki, R. Muller, F. McLarnon, J. Electrochem. Soc. 152 (2005) A774–A777.
[37] J. Mizusaki, H. Tagawa, K. Saito, K. Uchida, M. Tezuka, Solid State Ionics 53–56 (Part 2) (1992) 791–797.
[38] J. Park, J.H. Seo, G. Plett, W. Lu, A.M. Sastry, Electrochem. Solid State Lett. 14 (2011) A14–A18.
[39] W.B. Gu, C.Y. Wang, Lithium batteries, in: Proceedings of the International Symposium, 17-22 Oct. 1999, Electrochem. Soc, 2000, pp. 748–762. Pennington, NJ, USA.
[40] R. Spotnitz, J. Power Sources 113 (2003) 72–80.
[41] M. Doyle, J. Newman, A.S. Gozdz, C.N. Schmutz, J.M. Tarascon, J. Electrochem. Soc. 143 (1996) 1890–1903.
[42] Y. Ye, Y. Shi, N. Cai, J. Lee, X. He, J. Power Sources 199 (2012) 227–238.
[43] S.-B. Lee, S.-I. Pyun, Carbon 40 (2002) 2333–2339.